Strong-field ionization of atoms beyond the dipole approximation

D. Habibović [1] and D. B. Milošević [1,2,3,*]

[1] *University of Sarajevo, Faculty of Science, Zmaja od Bosne 33–35, 71000 Sarajevo, Bosnia and Herzegovina*

[2] *Academy of Sciences and Arts of Bosnia and Herzegovina, Bistrik 7, 71000 Sarajevo, Bosnia and Herzegovina*

[3] *Max-Born-Institut for Nonlinear Optics and Short Pulse Spectroscopy, Max-Born-Strasse 2a, 12489 Berlin, Germany*

(Received 13 July 2022; accepted 24 August 2022; published 2 September 2022)

Strong-field ionization of atoms by an elliptically polarized laser field is discussed beyond the dipole approximation. We develop a theory based on the strong-field approximation which includes nondipole effects by expanding vector potential up to the first order in $1/c$. Both direct and rescattered electrons are investigated. The differential ionization rate is calculated numerically or using the saddle-point method. We find that nondipole effects are mostly pronounced in the regions near and beyond the cutoff. The existence of additional regions in the photoelectron momentum plane where nondipole effects are significant is explained using the saddle-point method and the interference of partial contributions of particular saddle-point solutions to the differential ionization rate, which is modified when nondipole effects are taken into consideration. These regions are well defined for a linearly polarized field as well as for an elliptically polarized field with ellipticity lower than 0.4. For the rescattered electrons we find saddle-point solutions which contribute significantly to the differential ionization rate. These solutions are classified in a similar way as in the framework of the dipole approximation. The agreement of the results obtained by numerical integration and the results obtained using the saddle-point method is excellent.

DOI: 10.1103/PhysRevA.106.033101

I. INTRODUCTION

During the past decades dipole approximation has been employed to describe various strong-field processes such as high-order above-threshold ionization (HATI) and high-order harmonic generation [1]. This approximation assumes that the laser field is described by a spatially homogeneous electric field and vector potential so that the corresponding magnetic field is zero [2]. The laser-field parameters typical for the Ti:sapphire laser systems (wavelength around 800 nm and intensity of the order of 10^{14} W/cm^2), which have been employed to induce various atomic processes, are usually such to allow the use of the dipole approximation. However, laser systems with parameters for which this approximation is not adequate are now easily available. These systems typically have longer wavelength and higher intensity than that of the Ti:sapphire laser (see Fig. 2 in [3]). To assess whether the magnetic-field component should be taken into consideration it is useful to introduce the parameters z_f and β_0 [4,5]

$$z_f = \frac{2U_p}{mc^2}, \quad \beta_0 \approx \frac{U_p}{2mc\omega}, \tag{1}$$

where U_p is the electron ponderomotive energy, m and c are the electron mass and the speed of light, respectively, while ω is the laser-field frequency. The parameter z_f determines whether the relativistic effects should be taken into consideration, while the parameter β_0 determines whether or not the dipole approximation is adequate. In more detail, $z_f = 1$ means that $2U_p$ is equal to the rest energy of the particle so that the condition for the process to be nonrelativistic is $z_f \ll 1$. On the other hand, β_0 has a dimension of length and is the amplitude of motion in the propagation direction. For $\beta_0 \gtrsim 1$ a.u. the influence of the magnetic field should be taken into consideration. In this paper we are interested in the nonrelativistic nondipole regime, i.e., the regime where $z_f \ll 1$ and $\beta_0 \gtrsim 1$ a.u. The approach based on the time-dependent Schrödinger equation (TDSE) is time consuming and the semi-analytical theories are beneficial. One such theory is based on the strong-field approximation (SFA), which assumes that the influence of the parent ion on the liberated electron is negligible until eventual rescattering. The nondipole effects can be introduced by using the expansion of the vector potential $\mathbf{A}(\mathbf{r}, t)$ up to the first order in $1/c$ [6], i.e., $\mathbf{A}(t - \hat{\mathbf{k}} \cdot \mathbf{r}/c) \approx \mathbf{A}(t) + (\hat{\mathbf{k}} \cdot \mathbf{r})\mathbf{E}(t)/c$, where $\hat{\mathbf{k}}$ is the unit vector in the propagation direction and $\mathbf{E}(t) = -d\mathbf{A}(t)/dt$. The first term $\mathbf{A}(t)$ corresponds to the dipole approximation, while the second term accounts for the nondipole nonrelativistic effects. The transition amplitude can be written in the form of the sum of the contributions which correspond to the direct and rescattered electrons. The direct electrons do not interact with the parent ion after they are liberated, while the rescattered electrons exhibit one rescattering of the parent ion. The mentioned nondipole effects are sometimes called magnetic nondipole effects. In addition to them, the electric nondipole effects also arise due to the position dependence of the electric field and affect the momenta of the electrons emitted in the strong-field ionization [7]. These effects are not elaborated on in this paper.

*Corresponding author: milo@bih.net.ba

The influence of the nondipole effects on the photoelectron momentum distribution was experimentally observed in [8–12] and the theories which include nondipole corrections were employed. For example, in [13] the influence of the magnetic field on the plateau height and the position of the cutoff was investigated, while the transfer of the momentum in the propagation direction to the photoelectrons was explored in [14]. Moreover, in [15,16] the HATI process beyond dipole approximation was investigated using the TDSE for the model atom and the H_2^+ ion, while in [17] the Hamiltonian of the charged particle in a laser field was analyzed in detail. Finally, the nonrelativistic theory which describes detachment of an electron from the negative ion taking into consideration the nondipole effects was recently formulated in [18]. The nondipole ionization induced by a circularly polarized pulse was investigated in Refs. [19–22]. Particularly, using the Coulomb-corrected nondipole molecular SFA the photoelectron momentum distribution and the role of the degeneracy of the molecular orbitals was investigated in [21], while in [22] the nondipole under-the-barrier dynamics of the electron during strong-field tunneling ionization was explored by investigating the role of the Coulomb field of the atomic core.

In this paper we formulate the nonrelativistic theory of strong-field ionization that includes nondipole corrections of the order of $1/c$ and apply it to the ionization of neutral atoms exposed to a strong elliptically polarized laser field. The transition amplitudes of the direct and rescattered electrons are calculated using numerical integration as well as using the saddle-point method. The main goal of this paper is to investigate how the nondipole contributions affect the photoelectron spectra and how well the spectra can be reproduced using the saddle-point method. We use He and Xe atoms with s and p ground states, respectively, as examples. In addition, using the parameter β_0 introduced above we investigate the dependence of the nondipole contributions on the applied-field parameters.

This article is organized as follows. In Sec. II we formulate the SFA theory which includes nondipole corrections. Also, we define the driving field and discuss the saddle-point method, which can be used to calculate approximately the differential ionization rate. In Sec. III we present our numerical results for the cases of linear and elliptical polarizations for both direct and rescattered electrons. There we discuss how the nondipole contribution affects the photoelectron momentum distributions. Finally, in Sec. IV we summarize our paper and state the main conclusions. Atomic units in which $c = 137.036$ a.u. are used throughout the paper.

II. THEORY

A. Strong-field approximation

The HATI theory, based on the strong-field approximation, presented in [1], can be generalized to include nondipole effects. The expansion of the vector potential

$$\mathbf{A}\left(t - \frac{\hat{\mathbf{k}}\cdot\mathbf{r}}{c}\right) \approx \mathbf{A}(t) + \frac{\hat{\mathbf{k}}\cdot\mathbf{r}}{c}\mathbf{E}(t), \tag{2}$$

requires the dipole interaction $\mathbf{r}\cdot\mathbf{E}(t)$ to be replaced by [6]

$$H_{\rm int}(t) = \mathbf{E}(t)\cdot\left(\mathbf{r} - i\frac{\hat{\mathbf{k}}\cdot\mathbf{r}}{c}\nabla\right). \tag{3}$$

Additionally, the Volkov states are replaced by

$$|\chi_{\mathbf{p}}(t)\rangle = |\mathbf{q}_{\mathbf{p}}(t)\rangle e^{-iS_{\mathbf{p}}(t)}, \tag{4}$$

where

$$\mathbf{q}_{\mathbf{p}}(t) = \mathbf{p} + \mathbf{A}(t) + \hat{\mathbf{k}}[\mathbf{p}\cdot\mathbf{A}(t) + \mathbf{A}^2(t)/2]/c, \tag{5}$$

$$\begin{aligned} S_{\mathbf{p}}(t) &= \frac{1}{2}\int^t dt' \mathbf{q}_{\mathbf{p}}^2(t') \\ &= E_{\mathbf{p}}t + [\mathbf{p}\cdot\boldsymbol{\alpha}(t) + \mathcal{U}(t)](1 + \mathbf{p}\cdot\hat{\mathbf{k}}/c). \end{aligned} \tag{6}$$

Here $\boldsymbol{\alpha}(t) = \int^t dt'\mathbf{A}(t')$, $E_{\mathbf{p}} = \mathbf{p}^2/2$ is the photoelectron energy, and $\mathcal{U}(t) = \int^t dt'\mathbf{A}^2(t')/2 = U_p t + \mathcal{U}_1(t)$. For a $T = 2\pi/\omega$-periodic laser field, the differential ionization rate for the electron with momentum $\mathbf{p}$ and energy $E_{\mathbf{p}}$ is

$$w_{\mathbf{p}i}(n) = 2\pi p|T_{\mathbf{p}i}(n)|^2, \tag{7}$$

where n is the number of absorbed photons and the T-matrix element is $T_{\mathbf{p}i}(n) = T_{\mathbf{p}i}^{(0)}(n) + T_{\mathbf{p}i}^{(1)}(n)$. The contributions $T_{\mathbf{p}i}^{(0)}(n)$ and $T_{\mathbf{p}i}^{(1)}(n)$, in the SFA, are given by

$$T_{\mathbf{p}i}^{(0)}(n) = \int_0^T \frac{dt_0}{T}\langle\mathbf{q}_{\mathbf{p}}(t_0)|H_{\rm int}(t_0)|\psi_i\rangle e^{iS(\mathbf{p};t_0)}, \tag{8}$$

$$\begin{aligned} T_{\mathbf{p}i}^{(1)}(n) = -i\int_0^T \frac{dt}{T}\int_{-\infty}^t dt_0 \left[\frac{2\pi}{i(t-t_0)}\right]^{3/2} e^{iS_{\mathbf{p},\rm st}(t_0,t)} \\ \times \langle\mathbf{p} + \mathbf{p}\cdot\mathbf{A}(t)\hat{\mathbf{k}}/c|V(\mathbf{r})|\mathbf{K}_{\rm st} + \mathbf{K}_{\rm st}\cdot\mathbf{A}(t)\hat{\mathbf{k}}/c\rangle \\ \times \langle\mathbf{q}_{\mathbf{K}_{\rm st}}(t_0)|H_{\rm int}(t_0)|\psi_i\rangle, \end{aligned} \tag{9}$$

and they correspond to the direct and rescattered electrons, respectively. Here, $S(\mathbf{p};t_0) = S_{\mathbf{p}}(t_0) + I_p t_0$, with I_p the ionization potential and $\mathbf{K}_{\rm st}(t_0,t) = \mathbf{k}_{\rm st}(t_0,t) + \kappa(t_0,t)\hat{\mathbf{k}}/c$ with $\mathbf{k}_{\rm st}(t_0,t) = -\int_{t_0}^t dt'\mathbf{A}(t')/(t-t_0)$ and $\kappa(t_0,t) = \mathbf{k}_{\rm st}^2(t_0,t) - [\mathcal{U}_1(t) - \mathcal{U}_1(t_0)]/(t-t_0) - U_p$. Also,

$$S_{\mathbf{p},\rm st}(t_0,t) = S_{\mathbf{p}}(t) - \frac{1}{2}\int_{t_0}^t dt'\mathbf{q}_{\mathbf{K}_{\rm st}}^2(t') + I_p t_0, \tag{10}$$

where $|\psi_i\rangle$ is the initial bound state, and t_0 and t are the ionization and rescattering times, respectively. The rescattering potential is represented by the double Yukawa potential

$$V(r) = -\frac{Z}{H}\frac{e^{-r/D}}{r}[1 + (H-1)e^{-Hr/D}], \tag{11}$$

where $H = DZ^{0.4}$ and the values of D can be found in [23] for different noble gases. Using the double Yukawa potential we removed the singularity associated with the Coulomb potential, but also lost the long-range feature of the Coulomb potential.

The contributions $T_{\mathbf{p}i}^{(0)}(n)$ and $T_{\mathbf{p}i}^{(1)}(n)$, given by Eqs. (8) and (9), can be calculated numerically. The energy-conservation condition reads $n\omega = E_{\mathbf{p}} + I_p + U_p(1 + \mathbf{p}\cdot\hat{\mathbf{k}}/c)$, while the initial bound state can be written as $\psi_i(\mathbf{r}) \equiv \psi_{ilm}(\mathbf{r}) = R_{il}(r)Y_{lm}(\theta,\phi)$, where $Y_{lm}(\theta,\phi)$ are normalized spherical harmonics and the radial functions $R_{il}(r)$ are represented either as a linear combination of the Slater-type orbitals [24–27] or by the asymptotic wave functions [1,28]. In the first case, the radial wave function reads

$$R_{il}(r) = \sum_a c_a \frac{(2\zeta_a)^{n_a+1/2}}{\sqrt{(2n_a)!}} r^{n_a-1}e^{-\zeta_a r}, \tag{12}$$

where the parameters c_a and ζ_a characterize the radial electron probability density distribution, while the n_a and l are the quantum numbers. In the second case, the radial wave function is

$$R_{il}(r) \approx A r^{\nu-1} e^{-\kappa_0 r}, \quad r \gg 1, \tag{13}$$

where $\nu = 1/\kappa_0$, $\kappa_0 = \sqrt{2I_p}$ and the constant A can be found in [27]. This approximation is appropriate for large distances r [28].

To quantify the influence of the nondipole effects on the differential ionization rate we introduce the parameter $\delta_{\mathbf{p}i}(n)$,

$$\delta_{\mathbf{p}i}(n) = \frac{w^{\rm nd}_{\mathbf{p}i}(n) - w^{\rm dip}_{\mathbf{p}i}(n)}{w^{\rm nd}_{\mathbf{p}i}(n) + w^{\rm dip}_{\mathbf{p}i}(n)}, \tag{14}$$

which represents the normalized difference between the differential ionization rates calculated using nondipole effects ("nd") and using the dipole approximation ("dip"). At the end of this subsection let us mention that the nondipole SFA theory was also established in [29,30] using different approaches.

B. Saddle-point method

In the present paper, we analyze the case of a field with parameters for which nondipole effects have to be taken into consideration. In particular, we analyze the elliptically polarized field of the form

$$\mathbf{E}(t) = \frac{E}{\sqrt{1+\varepsilon^2}}[\sin(\omega t)\hat{\mathbf{e}}_x - \varepsilon\cos(\omega t)\hat{\mathbf{e}}_y], \tag{15}$$

where E, ε, and ω are the laser field amplitude, ellipticity, and frequency, respectively, and the propagation direction is $\hat{\mathbf{e}}_z = \hat{\mathbf{k}}$, with $\hat{\mathbf{e}}_x$, $\hat{\mathbf{e}}_y$, and $\hat{\mathbf{e}}_z$ the unit vectors. We determine the photoelectron momentum in the $p_z p_x$ plane, using the momentum-space spherical coordinates. The corresponding azimuthal angle is $\varphi = 0^\circ$, while the polar angle θ is the electron emission angle.

The integral which appears in Eq. (8) can be solved approximately using the saddle-point (SP) method. The condition $dS(\mathbf{p};t_0)/dt_0 = 0$ leads to the SP equation $\mathbf{q}^2_{\mathbf{p}}(t_0) = -2I_p$ which, neglecting the term proportional to $1/c^2$, can be written as

$$\{\mathbf{p}^2 + \mathbf{A}^2(t_0) + 2\mathbf{p}\cdot\mathbf{A}(t_0) + 2p_z[\mathbf{p}\cdot\mathbf{A}(t_0) + \mathbf{A}^2(t_0)/2]/c\}^2 = -2I_p, \tag{16}$$

and represents the energy-conservation condition at the ionization time. For the initial state represented by the asymptotic wave function, the direct-electron contribution becomes [28,31]

$$T^{(0),\rm SP}_{\mathbf{p}i}(n) = i2^{-3/2}T^{-1}A\kappa_0^{\nu}\nu\Gamma(\nu/2) \times \sum_{t_{0s}} \left(\frac{q_s}{i\kappa_0}\right)^l Y_{lm}(\hat{\mathbf{q}}_{\mathbf{p}s}) e^{iS_s} \left(\frac{2i}{S''_s}\right)^{(\nu+1)/2}, \tag{17}$$

where the sum over t_{0s} is the sum over the solutions of the SP Eq. (16), located in the upper half of the complex plane, $\mathbf{q}_{\mathbf{p}s} \equiv \mathbf{q}_{\mathbf{p}}(t_{0s})$, $S_s \equiv S(\mathbf{p};t_{0s})$, and

$$S''_s \equiv \frac{d^2S(\mathbf{p};t_{0s})}{dt_0^2} = -\mathbf{q}_{\mathbf{p}}(t_{0s})\cdot\{\mathbf{E}(t_{0s}) + \mathbf{E}(t_{0s})\cdot[\mathbf{p} + \mathbf{A}(t_{0s})]\hat{\mathbf{k}}/c\}. \tag{18}$$

On the other hand, for the rescattered electrons the stationarity conditions $\partial S_{\mathbf{p},\rm st}(t_0,t)/\partial t_0 = 0$ and $\partial S_{\mathbf{p},\rm st}(t_0,t)/\partial t = 0$ lead to the SP equations $\mathbf{q}^2_{\mathbf{K}_{\rm st}}(t_0) = -2I_p$ and $\mathbf{q}^2_{\mathbf{K}_{\rm st}}(t) = \mathbf{q}^2_{\mathbf{p}}(t)$. Using Eq. (5) and neglecting the terms proportional to $1/c^2$ these equations become

$$[\mathbf{k}_{\rm st} + \mathbf{A}(t_0)]^2 = -2I_p, \tag{19}$$

$$[\mathbf{k}_{\rm st} + \mathbf{A}(t)]^2 = \{\mathbf{p}^2 + \mathbf{A}^2(t) + 2\mathbf{p}\cdot\mathbf{A}(t) + 2p_z[\mathbf{p}\cdot\mathbf{A}(t) + \mathbf{A}^2(t)/2]/c\}^2, \tag{20}$$

and represent the energy-conservation conditions at the ionization and rescattering times, respectively. Equation (19) is the same as in the dipole approximation, while Eq. (20) is modified by the nondipole effects with respect to the corresponding equation obtained using the dipole approximation. The modified SP method leads to the following expression for the rescattering T-matrix element [31]:

$$T^{(1),\rm SP}_{\mathbf{p}i}(n) = \pi^2 T^{-1} A\kappa_0^{\nu}\nu\Gamma(\nu/2) \sum_{\{t_{0s},t_s\}} \left(\frac{q_{\mathbf{K}_{\rm st}s}}{i\kappa_0}\right)^l e^{iS_{{\rm st},s}} \times Y_{lm}(\hat{\mathbf{q}}_{\mathbf{K}_{\rm st}s}) \frac{\langle\mathbf{p}|V|\mathbf{k}_{\rm st}\rangle}{[i(t_s - t_{0s})]^{3/2}} \times \left(\frac{2i}{S''_{{\rm st}0,s}}\right)^{(\nu+1)/2} \left(\frac{2i}{S''_{{\rm st},s}}\right)^{1/2}, \tag{21}$$

where $\mathbf{q}_{\mathbf{K}_{\rm st}s} \equiv \mathbf{q}_{\mathbf{K}_{\rm st}}(t_{0s})$, $S_{{\rm st},s} \equiv S_{\mathbf{p},\rm st}(t_{0s},t_s)$, $S''_{{\rm st}0,s} \equiv \partial^2 S_{\mathbf{p},\rm st}(t_0,t)/\partial t_0^2|_{t_{0s},t_s}$, and $S''_{{\rm st},s} \equiv \partial^2 S_{\mathbf{p},\rm st}(t_0,t)/\partial t^2|_{t_{0s},t_s}$.

The solutions of the SP Eqs. (19) and (20) in the dipole approximation were analyzed in [31–35] for the linearly polarized field and for the bicircular field.

Before we proceed and present our numerical results, let us investigate the number of solutions of Eq. (16) for our elliptically polarized field. Neglecting the term proportional to $1/c^2$, the SP Eq. (16) can be written in the form $\mathbf{q}^2_{\mathbf{p}}(t_0) + 2I_p = 0$, with

$$\mathbf{q}^2_{\mathbf{p}}(t_0) + 2I_p = \sum_{k=0}^{2} a_k\cos(k\omega t_0) + \sum_{k=1}^{2} b_k\sin(k\omega t_0). \tag{22}$$

Using the substitution $z = e^{i\omega t_0}$ and the exponential forms of the sine and cosine functions, the trigonometric polynomial (22) can be rewritten as $\mathbf{q}^2_{\mathbf{p}}(t_0) + 2I_p = z^{-2}F(z)$ where the function $F(z)$ is the polynomial of the order four [32,36,37],

$$F(z) = \sum_{k=0}^{4} c_k z^k, \tag{23}$$

with $c_2 = a_0$ and $c_k = c^*_{4-k} = (a_{2-k} + ib_{2-k})/2$, $k = 0, 1$. This polynomial has four complex zeros provided $c_4 \neq 0$, while the corresponding zeros of the polynomial $\mathbf{q}^2_{\mathbf{p}}(t_0) + 2I_p$ are

$$\omega t_{0k} = -i\ln z_k, \quad 0 \leqslant \mathrm{Re}\,\omega t_{0k} < 2\pi, \quad k = 1,\ldots,4. \tag{24}$$

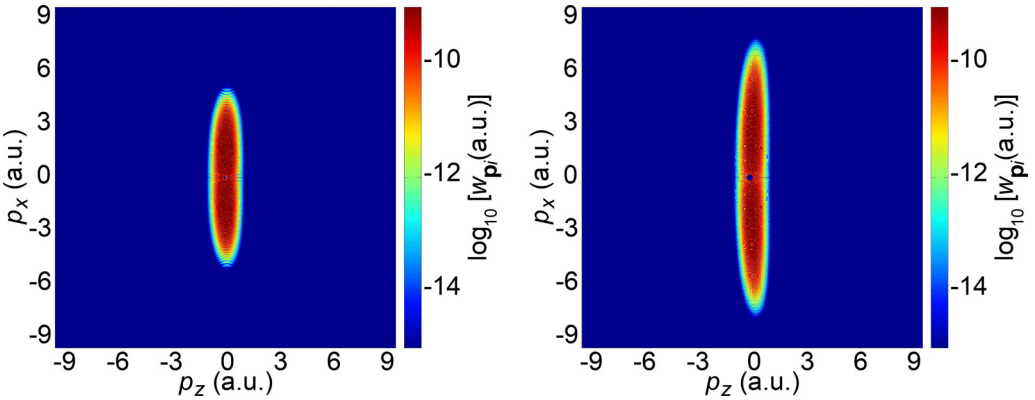

FIG. 1. Logarithm of the differential ionization rate of He atom presented in false colors in the photoelectron momentum plane for the case of ionization by a linearly polarized field with intensity $I = E^2 = 5\times10^{14}$ W/cm^2. The values of the wavelength λ and parameter β_0 are λ = 2000 nm, $\beta_0 = 1.1$ a.u. (left panel), and λ = 3200 nm, $\beta_0 = 4.51$ a.u. (right panel).

For every solution ωt_0, its complex conjugate ωt_0^* is also a solution. However, for the application of the SP method we only take into account the two solutions in the upper half of the complex plane. The differential ionization rate

$$w_{\mathbf{p}i}^{ab}(n) \propto |ae^{iS_a} + be^{iS_b}|^2, \quad S_j = S(\mathbf{p}, t_{0j}), \quad j = a, b, \quad (25)$$

which corresponds to these solutions (denoted by the labels "a" and "b") can be written as [38]

$$w_{\mathbf{p}i}^{ab}(n) \propto |a|^2 e^{-2\,\mathrm{Im}\,S_a}\{1 + |\mathcal{A}|^2 + 2|\mathcal{A}| \times \sin[\mathrm{Re}(S_a - S_b) + \arcsin(\mathrm{Re}\,\mathcal{A}/|\mathcal{A}|)]\}, \quad (26)$$

where $\mathcal{A} = b\exp[\mathrm{Im}(S_a - S_b)]/a$. Finally, it is instructive to mention that if the term proportional to $1/c^2$ is taken into account, Eq. (16) has four instead of two relevant solutions. This term is significant for a very strong laser field when the relativistic effects have to be taken into consideration.

III. NUMERICAL RESULTS

In this section we present our numerical results using the examples of He and Xe atoms exposed to the laser field with parameters for which the dipole approximation is questionable. The intensity of the applied field is such that the saturation effects and the depletion of the ground state do not have to be taken into consideration. The helium (xenon) atom has $1s$ ($5p$) ground state so that the magnetic quantum number is $m = 0$ ($m = 0, \pm1$).

A. Direct photoelectron spectra

We start with the example of He atoms exposed to the linearly polarized field ($\varepsilon = 0$). In Fig. 1 we present the photoelectron momentum distributions obtained by exposing He atoms to the linearly polarized field with intensity $I = 5\times10^{14}$ W/cm^2. The values of the wavelength are 2000 nm (left panel) and 3200 nm (right panel), while the corresponding values of the parameter β_0 are 1.1 a.u. (left panel) and 4.51 a.u. (right panel). The values of the parameter β_0 are larger than 1 a.u. and the dipole approximation is questionable. The photoelectrons are predominantly emitted in the field polarization direction even though the distribution is slightly tilted towards the positive values of p_z. This alteration becomes more pronounced for larger values of β_0 as we shall discuss later. Before that, let us first analyze the influence of the nondipole effects on the differential ionization rate for different values of the photoelectron energy and emission angle. To do that, in Fig. 2 we present the parameter $\delta_{\mathbf{p}i}(n)$, given by Eq. (14), in the photoelectron momentum plane for the same laser-field parameters as in Fig. 1. The first obvious observation is that the nondipole effects are crucial for the energy close to and beyond the point after which the differential ionization rate drops significantly. However, it is also evident that the nondipole effects are significant for some lower values of the energy for which the differential ionization rate is high. For example, in the left panel of Fig. 2, for $p_z > 0$ two parentheses-like structures are clearly visible and represent the regions in the photoelectron momentum plane where the nondipole effects are significant. The first structure extends from $(p_z, p_x) = (1.5$ a.u., -5.5 a.u.) to $(p_z, p_x) = (1.5$ a.u., 5.5 a.u.), while the second one is located closer to the cutoff position, i.e., from $(p_z, p_x) = (2$ a.u., -3 a.u.) to $(p_z, p_x) = (2$ a.u., 3 a.u.). Similar structures are also present for $p_z < 0$. Comparing the left panels of Figs. 1 and 2 it is evident that the differential ionization rate is significant along the observed parentheses-like structures. For the larger values of β_0, the number of these structures increases and already for $\beta_0 = 4.51$ a.u. the nondipole effects should be taken into consideration for most values of the photoelectron energy and emission angle. Moreover, let us mention that the larger value of the parameter z_f would be more beneficial for generating the asymmetry in the photoelectron momentum distribution. However, for the laser-field parameters examined in this paper $z_f \ll 1$, i.e., the relativistic effects are negligible.

To explain these structures, we use the saddle-point method. For illustration we use the example for which $\beta_0 = 1.1$ a.u. The corresponding photoelectron momentum distribution and $\delta_{\mathbf{p}i}(n)$ are shown in the left panels of Figs. 1 and 2, respectively. Solving Eq. (16) we obtain two complex solutions t_{0s} in the upper-half of the complex plane. With these solutions we calculate the corresponding value of the direct T-matrix element $T_{\mathbf{p}i}^{(0),\mathrm{SP}}(n)$ using Eq. (17) where $Y_{00} = 1/\sqrt{4\pi}$ and the corresponding differential ionization rate is

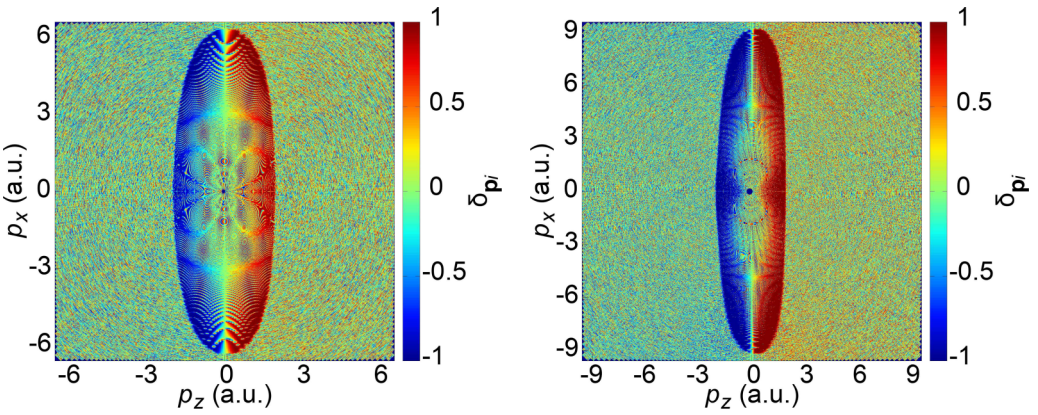

FIG. 2. Parameter $\delta_{\mathbf{p}i}(n)$ presented in false colors in the photoelectron momentum plane for He atom exposed to the same laser field as in Fig. 1.

given by Eq. (7). This procedure is done taking into account the nondipole effects as well as in the dipole approximation which allows one to calculate the corresponding value of the parameter $\delta_{\mathbf{p}i}(n)$ for different values of the photoelectron energy and emission angle. In Fig. 3 we present the differential ionization rate calculated using one solution (upper left panel) and both solutions (upper right panel) of the SP Eq. (16), while the corresponding results for the parameter $\delta_{\mathbf{p}i}(n)$ are presented in the lower panels. Careful comparison of the results shown in the upper panels of Fig. 3 reveals that the oscillations of the differential ionization rate are caused by the interference of the two SP contributions to the differential ionization rate. The distributions shown in the left panels of Fig. 3 are smooth, while those shown in the right panels exhibit rapid oscillations. The oscillations of the differential ionization rate are fast so that the spectra look as averaged to one particular value. In addition, the result obtained using the SP method reproduces well the one obtained by numerical integration (compare the upper right panel of Fig. 3 and the left panel of Fig. 1). This is particularly important due to the fact that the numerical calculations for the laser-field parameters for which nondipole effects are significant are often time

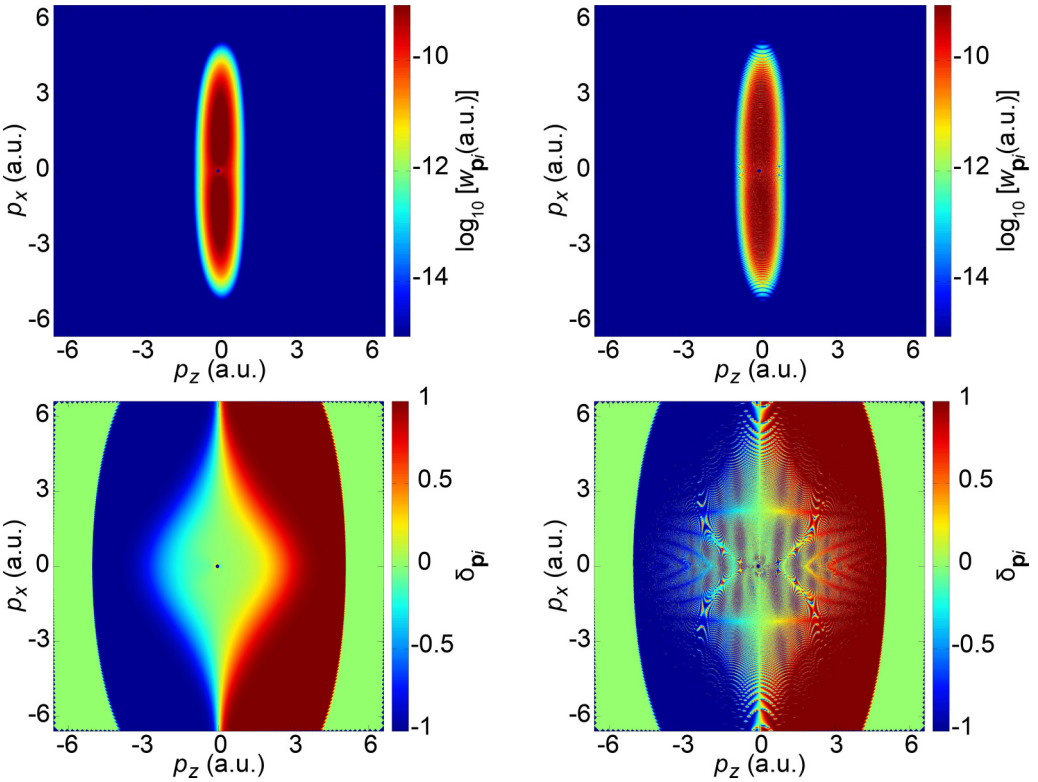

FIG. 3. Upper row: Logarithm of the differential ionization rate of the He atom presented in false colors in the photoelectron momentum plane for the case of ionization by a linearly polarized field, calculated using one solution (left panel) and both solutions (right panel) of the SP Eq. (16). Lower row: The corresponding parameter $\delta_{\mathbf{p}i}(n)$ presented in false colors in the photoelectron momentum plane calculated using one solution (left panel) and both solutions (right panel) of the SP Eq. (16). Laser-field parameters are the same as in the left panel of Fig. 1.

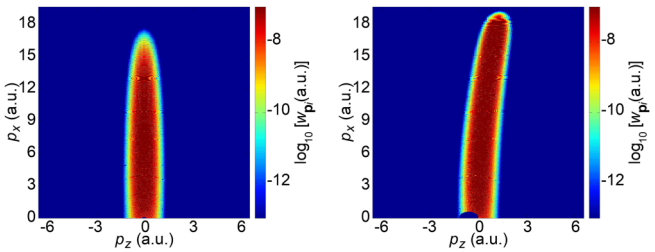

FIG. 4. Logarithm of the differential ionization rate of the He atom presented in false colors in the photoelectron momentum plane for the case of ionization by a linearly polarized field with intensity $I = 1.5\times10^{15}$ W/cm^2 and wavelength 4000 nm. The corresponding value of the parameter β_0 is $\beta_0 = 26.42$ a.u. The results in the left panel are obtained using the dipole approximation, while the results in the right panel include nondipole effects.

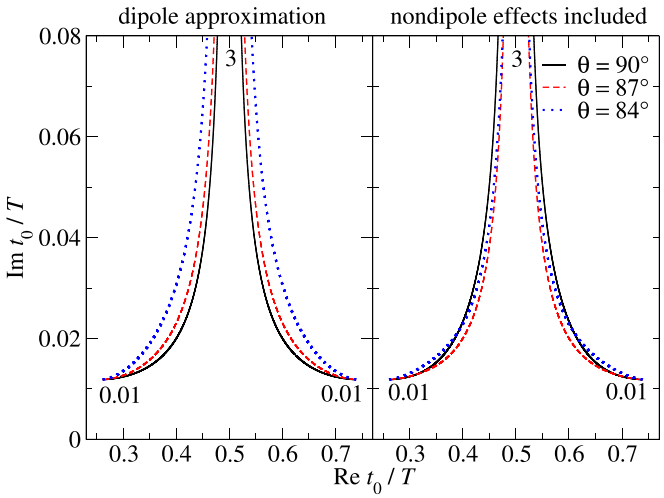

FIG. 5. Saddle-point solutions for the complex ionization time t_0 for the He atom, exposed to a linearly polarized field with the same parameters as in Fig. 4, calculated using the dipole approximation (left panel) and taking into account nondipole effects (right panel). The values of the emission angle are indicated in the legend. The photoelectron energy changes from $0.01U_p$ to $3U_p$ along each curve as indicated.

consuming. Furthermore, regarding the parameter $\delta_{\mathbf{p}i}(n)$, it is clear that the parentheses-like structure obtained using numerical integration is well reproduced using the SP method (compare the lower right panel of Fig. 3 and the left panel of Fig. 2). This structure is absent if only one quantum orbit is taken into account (see the lower left panel of Fig. 3), indicating that the interference of the two SP contributions is influenced by the nondipole effects. This dependence causes the earlier-noticed parentheses-like structures. Finally, let us mention that the parentheses-like regions where the nondipole effects are significant (see Fig. 2 and the lower right panel of Fig. 3) are quantitatively changed when the rescattered electrons are taken into consideration. This particularly happens for the values of the photoelectron energy close and beyond the cutoff energy of the direct electrons due to the interference of the direct and rescattered contributions to the T-matrix element. The photoelectron momentum distributions similar to those shown in our previously discussed figures were also analyzed in [39,40]. In more detail, in [39] the tunneling dynamics was investigated using the relativistic SFA theory, while in [40] the dependence of the radiation pressure on photoelectrons on the details of the ionization mechanism was explored.

Let us discuss in more detail the effects of nondipole contributions on the shape of the photoelectron momentum distribution and the position of the cutoff. In Fig. 4, for the He atoms exposed to a linearly polarized field with intensity $I = 1.5\times10^{15}$ W/cm^2 and wavelength 4000 nm, we present the photoelectron momentum distribution for $p_x > 0$. Helium atom has large ionization potential so that such high intensity still does not require inclusion of the saturation effects. The corresponding value of the parameter β_0 is $\beta_0 = 26.42$ a.u. For a given value of the emission angle, the position of the cutoff is changed when the nondipole effects are included. In particular, in the framework of the dipole approximation, the photoelectrons with highest energy can be expected in the direction of the driving-field polarization, which is not the case when the differential ionization rate is calculated using the nondipole SFA theory. Additionally, in the nondipole SFA case the photoelectrons with higher energy can be expected.

To discuss this point in more detail we use the SP method. The imaginary part of the ionization time t_0 is related to the ionization probability. In particular, the subintegral function in the action $S(\mathbf{p}; t_{0s})$ contains the term $\mathbf{q}^2_{\mathbf{p}}(t')$, which can be approximated using the first three terms of the Taylor expansion about the point $t_{0s\mathrm{R}} = \mathrm{Re}\, t_{0s}$:

$$\mathbf{q}^2_{\mathbf{p}}(t') \approx \mathbf{q}^2_{\mathbf{p}}(t_{0s\mathrm{R}}) + \partial\mathbf{q}^2_{\mathbf{p}}(t')/\partial t'|_{t'=t_{0s\mathrm{R}}}(t' - t_{0s\mathrm{R}}) + \tfrac{1}{2}\partial^2\mathbf{q}^2_{\mathbf{p}}(t')/\partial t'^2|_{t'=t_{0s\mathrm{R}}}(t' - t_{0s\mathrm{R}})^2. \quad (27)$$

Using Eq. (27) and the SP Eq. (16) the exponential term in Eq. (17) becomes

$$e^{iS(\mathbf{p};t_{0s})} = e^{iS(\mathbf{p};t_{0s\mathrm{R}})}e^{-[\mathbf{q}^2_{\mathbf{p}}(t_{0s\mathrm{R}})+2I_p]t_{0s\mathrm{I}}/3}, \quad (28)$$

where $t_{0s\mathrm{I}}$ is the imaginary part of the ionization time. The ionization probability decreases exponentially with the increase of $t_{0s\mathrm{I}}$. In Fig. 5 we present two SP solutions for the ionization time t_0 (in units of the optical period T), for the values of the emission angle as indicated in the legend, calculated in the framework of the dipole approximation (left panel) and taking into account nondipole effects (right panel). The photoelectron energy on each curve changes continuously from $0.01U_p$ to $3U_p$. Even though in both cases the solutions are symmetric with respect to the $\mathrm{Re}\, t_0 = 0.5T$ line, their dependence on the angle θ is different. In the dipole approximation, the imaginary part of the ionization time increases as the angle θ decreases from 90°, leading to a decrease of the differential ionization rate. Even an alteration of the emission angle of only few degrees from $\theta = 90°$ leads to a drastic decrease of the differential ionization rate except for the low-energy electrons. This is in agreement with the results shown in the left panel of Fig. 4. On the other hand, when the nondipole effects are taken into account, the imaginary part of the time t_0 (for a fixed energy) first decreases and then increases with the decrease of the angle θ from 90° (see the right panel of Fig. 5). As a result, the differential ionization rate is maximal for the emission angle $\theta \neq 90°$. Both SP solutions are affected in the

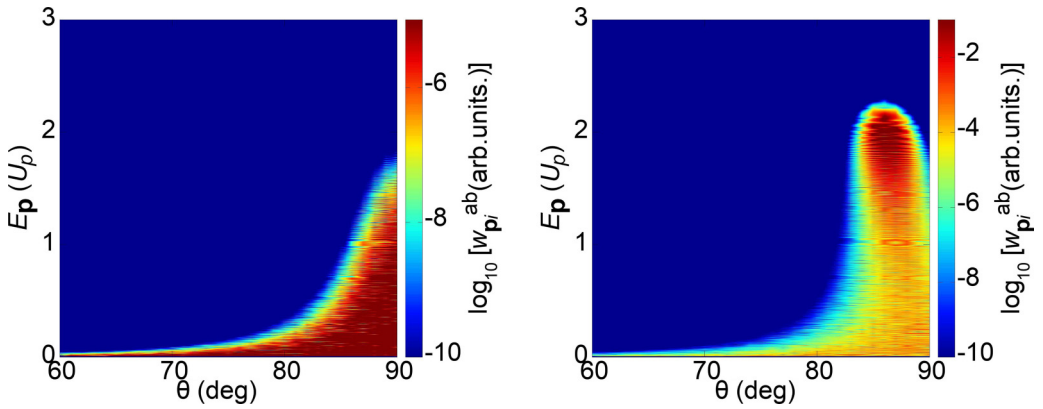

FIG. 6. Logarithm of the contribution $w_{\mathbf{p}i}^{ab}(n)$ to the differential ionization rate as a function of the emission angle and photoelectron energy calculated using the dipole approximation (left panel) and including nondipole effects (right panel) for the He atom exposed to a linearly polarized field with the same parameters as in Fig. 4.

same way by the nondipole effects. This can be elaborated further using the fact that Eq. (16) has only two solutions and that the differential ionization rate can be estimated using Eq. (26). Assuming that the contributions of the two SP solutions are equal, the differential ionization rate can be estimated for the given photoelectron energy and emission angle. In Fig. 6 we present the logarithm of the contribution $w_{\mathbf{p}i}^{ab}(n)$ to the differential ionization rate as a function of the emission angle and photoelectron energy using the dipole approximation (left panel) and including nondipole effects (right panel). The results obtained using the dipole approximation show that the contribution $w_{\mathbf{p}i}^{ab}(n)$ rapidly decreases as the emission angle decreases from $\theta = 90^\circ$ for all photoelectrons except those with very low energy. Beyond the dipole approximation this distribution is altered in such a way that the contribution $w_{\mathbf{p}i}^{ab}(n)$ exhibits maximum for the emission angle $\theta \neq 90^\circ$. In addition, the position of the cutoff is shifted towards higher energy. This significant change induced by nondipole effects steams from the fact that the quantity $\mathrm{Re}(S_a - S_b)$, which appears in the second line of Eq. (26), strongly depends on the nondipole contributions, particularly for energy $E_{\mathbf{p}} > 0.8U_p$. This change is qualitatively the same for a broad range of values of the parameter β_0.

In conclusion, the nondipole effects alter the shape of the photoelectron spectra as well as the position of the cutoff. This is particularly pronounced for the values $\beta_0 > 20$ a.u. On the other hand, for smaller values of this parameter the nondipole effects are significant for some values of the photoelectron energy and emission angle as explained using the SP method. In short, these effects exert influence on the interference of the partial contributions to the differential ionization rate.

Similar conclusions hold for other noble gases and an elliptically polarized field. For illustration, in Fig. 7 we present the photoelectron momentum distribution for Xe atoms exposed to an elliptically polarized field with ellipticity $\varepsilon = 0.25$ (top left panel), $\varepsilon = 0.35$ (middle left panel), and $\varepsilon = 0.5$ (bottom left panel) together with the corresponding values of the parameter $\delta_{\mathbf{p}i}(n)$ (right column). The photoelectron momentum distribution is obtained using nondipole SFA theory.

For the elliptically polarized field with ellipticity $\varepsilon = 0.25$ the photoelectron momentum distribution has a similar shape as the one obtained using a linearly polarized field. One obvious difference is that the photoelectrons with low and medium energy emitted in the direction $\theta = 90^\circ$ are suppressed to some extent (see the top left panel of Fig. 7) in comparison with those obtained using a linearly polarized field. The parameter $\delta_{\mathbf{p}i}(n)$ behaves in a similar way as for the linearly polarized field. For the elliptically polarized field with ellipticity $\varepsilon = 0.35$, the suppression of the low- and medium-energy electrons is even more pronounced. The earlier-discussed structures which appear when the parameter $\delta_{\mathbf{p}i}(n)$ is presented in the photoelectron momentum plane are still visible, but now they rather have an erratic form due to the fact that the differential ionization rate is low regardless of whether nondipole effects are taken into account or not. In this case, even the electrons with the energy close to the cutoff are significantly suppressed (cf. the false color scales in the top and middle left panels of Fig. 7). Finally, the bottom left panel shows the photoelectron momentum distribution for the elliptically polarized field with ellipticity $\varepsilon = 0.5$. The shape of the spectra is similar to the one obtained using a circularly polarized field [18] and the differential ionization rate of the high-energy electrons is significantly higher than for the case of the field with ellipticity $\varepsilon = 0.35$. The corresponding parameter $\delta_{\mathbf{p}i}(n)$ shown in the bottom right panel of Fig. 7 exhibits little or no structure and the only important information which can be extracted is that the nondipole effects are mostly pronounced in the close proximity of the cutoff. The nondipole ionization induced by an elliptically polarized pulses was also investigated in [41] where field-induced momentum transfer is explored as a function of the properties of the ultrashort laser pulse and in [42] where the electron nondipole dynamics was investigated using a relativistic Coulomb-corrected SFA based on the eikonal approximation of the Klein-Gordon equation.

B. Rescattered photoelectron spectra

After analyzing direct photoelectron spectra let us now devote our attention to the rescattered electrons. The calculations which have to be done to obtain the corresponding spectra are time consuming even for the driving-field parameters for which $\beta_0 \approx 1$ a.u. so that the SP method is particularly desirable. As an example, we use the He atom

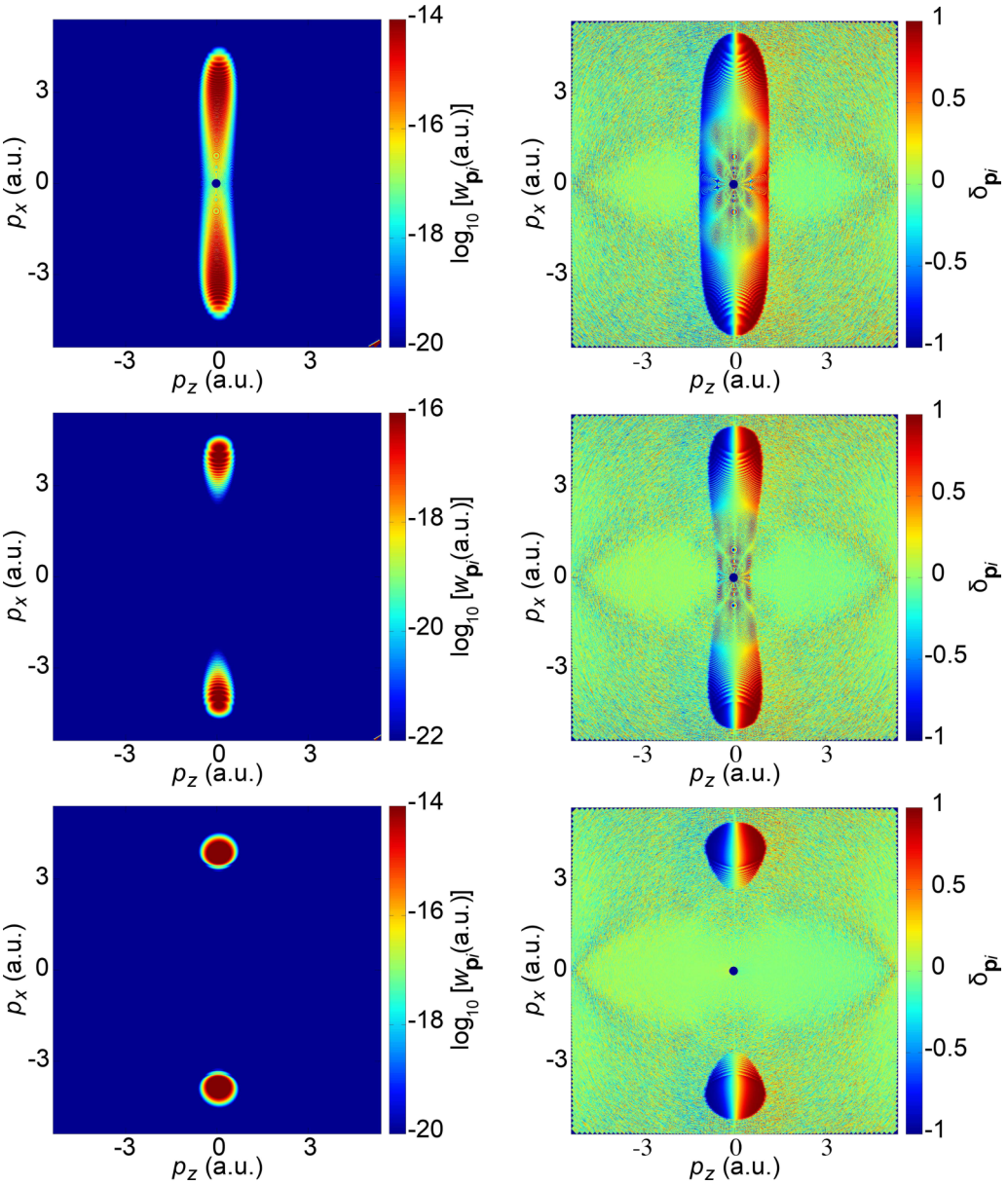

FIG. 7. Logarithm of the differential ionization rate (left column) and corresponding parameter $\delta_{\mathbf{p}i}(n)$ (right column) of the Xe atom, presented in false colors in the photoelectron momentum plane for the case of ionization by an elliptically polarized field with ellipticity $\varepsilon = 0.25$ (top row), $\varepsilon = 0.35$ (middle row), and $\varepsilon = 0.5$ (bottom row). The field intensity and wavelength are $I = 10^{14}$ W/cm^2 and $\lambda = 3500$ nm, respectively.

exposed to a linearly polarized field with the same parameters as in the left panel of Fig. 1. For the rescattered electrons the SP equations are given by Eqs. (19) and (20). If we restrict the rescattering time $0 < \mathrm{Re}\, t < T$ and solve the system of Eqs. (19) and (20) we get the so-called backward-scattering solutions which are mostly dominant in the medium- and high-energy part of the spectra. For a linearly polarized field, in the framework of the dipole approximation these solutions can be classified using the multi-index (α, β, m) [43]. The same classification can also be used when nondipole effects are taken into consideration. The solutions appear in pairs. The index $m = 0, 1, \ldots,$ counts the approximate length of the travel time $\mathrm{Re}(t - t_0)$ in the multiples of the field period T, while the index β counts the solutions within one optical cycle characterized by the index m. Finally, the index α serves to distinguish solutions of one pair, i.e., the so-called long and short orbits [44]. In Fig. 8 we present the solutions of the system of the SP Eqs. (19) and (20) for the emission angle $\theta = 90^\circ$ and the same field parameters as in the left panel of Fig. 1. In the left (right) panel the photoelectron energy $E_{\mathbf{p}}$ is presented as a function of the real part of the ionization (rescattering) time. For a given value of the index m there are two pairs of the backward-scattering solutions with different values of the index α. The contribution of one of the $\alpha = \pm 1$ solutions is divergent after the cutoff where it should be disregarded (this problem can be solved using the uniform approximation [43–45]). The partial contributions of the (α, β, m) solutions to the differential ionization rate

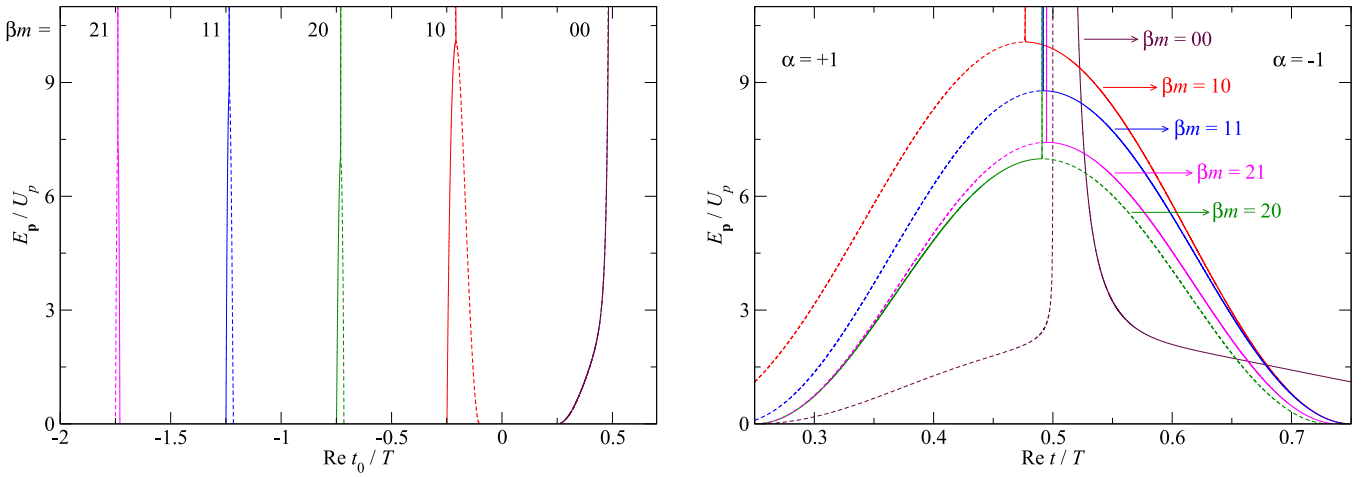

FIG. 8. Solutions of the system of the SP Eqs. (19) and (20) for a linearly polarized field beyond the dipole approximation for the same parameters as in the left panel of Fig. 1. The emission angle is $\theta = 90^\circ$. In the left (right) panel the photoelectron energy $E_{\mathbf{p}}$ is presented as a function of the real part of the ionization (rescattering) time.

are shown in the left panel of Fig. 9, while the comparison of the SP result with the one calculated using the numerical integration is presented in the right panel of Fig. 9. The contribution of the solution $(\beta, m) = (1, 0)$ is significant for all values of the photoelectron energy, while the solution $(\beta, m) = (2, 0)$ is significant for the energy lower than 7.3 U_p. On the other hand, the contributions of the solutions $(\beta, m) = (1, 1)$ and $(\beta, m) = (2, 1)$ are large only for some narrow energy regions. Finally, the solution $(\beta, m) = (0, 0)$ contributes only in the low-energy part of the spectra. The results obtained by numerical integration are well reproduced using the SP method for all values of the photoelectron energy, as can be seen in the right panel of Fig. 9.

In the end, let us compare the differential ionization rates of the rescattered electrons obtained in the dipole approximation with those obtained including nondipole effects. For this purpose we use the SP method. In Fig. 10 we present the logarithm of the differential ionization rate as a function of the photoelectron energy calculated using the dipole approximation (black solid line) and taking into account nondipole effects (red dashed line). The emission angle is $\theta = 87^\circ$. Contrary to the case of the direct electrons, for the rescattered electrons the position of the cutoff changes only slightly when the nondipole effects are taken into consideration. To explain this, we recall that the direct electrons are predominantly emitted in the direction of the applied field, while the differential ionization rate of the rescattered electrons is significant for a broad range of values of the photoelectron momentum (see Fig. 6 in [18]). As a result, the photoelectron momentum spectra would be tilted towards the positive values of p_z, but the position of the cutoff would not be changed a lot. Besides the cutoff region, the nondipole effects can affect other parts of the photoelectron energy spectra as well, provided $\beta_0 > 1$ a.u. In the case of the example shown in Fig. 10 it is obvious that the nondipole effects alter the contribution of the $(\beta, m) = (0, 0)$ solution which is dominant in the low-energy

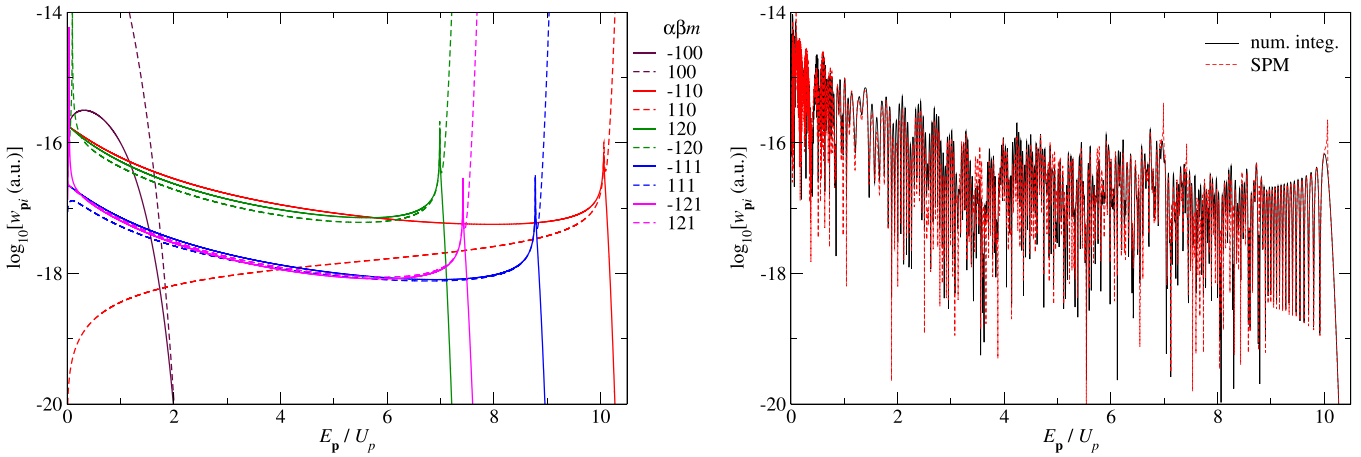

FIG. 9. Left panel: Partial contributions of the backward-scattering SP solutions, shown in Fig. 8, to the differential ionization rate. Right panel: Comparison of the rescattered photoelectron spectra obtained by using the numerical integration (black solid line) and the SP method (red dashed line).

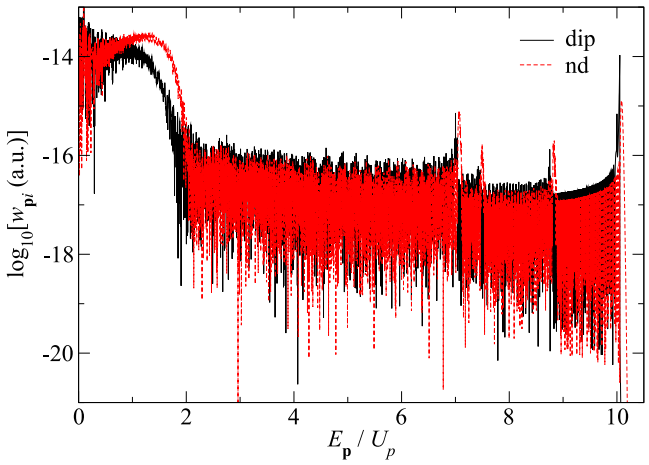

FIG. 10. Comparison of the rescattered photoelectron spectra of the He atom obtained by using the dipole approximation (black solid line) and including nondipole effects (red dashed line). The direct electrons are not taken into account. The emission angle is $\theta = 87^\circ$. The intensity of the applied field is $I = 1.5\times10^{15}$ W/cm^2, while the fundamental wavelength is 2600 nm.

part of the spectra. The influence of the nondipole effects on the other SP solutions is not so significant in this case.

IV. CONCLUSION

In this paper we generalized high-order above-threshold ionization theory based on the strong-field approximation so that the nondipole effects are taken into consideration. The integrals which appear in the corresponding expression for the differential ionization rate can be calculated numerically or using the saddle-point method. To determine whether or not nondipole effects should be taken into consideration we employed the parameter β_0 which represents the amplitude of the electron motion parallel to the field propagation direction.

First, we investigated the direct photoelectrons which after liberation do not interact with the parent ion. For a laser field polarized in the xy plane, the photoelectron momentum distribution in the $p_z p_x$ plane, obtained in the framework of the dipole approximation, exhibits reflection symmetry with respect to the $p_z p_y$ and $p_x p_y$ planes. When the nondipole effects are taken into consideration, the reflection symmetry with respect to the $p_x p_y$ plane is broken and the photoelectron momentum distribution is tilted towards the positive p_z part of the momentum plane. To quantitatively describe the intensity of nondipole effects, we introduced the parameter $\delta_{\mathbf{p}i}(n)$ which represents the normalized difference between the differential ionization rates calculated with and without nondipole effects. Presenting this parameter in the photoelectron momentum plane it becomes obvious that nondipole effects are most significant in the vicinity of the cutoff. In addition, the parentheses-like structures appear, defining the regions with large differential ionization rate in which these effects are nonnegligible. These structures appear for the values of the parameter β_0 close to 1 a.u. and they can be explained using the saddle-point method. In short, for an elliptically polarized field there are two solutions of the saddle-point equation for the direct electrons. The interference of these solutions is responsible for the oscillatory character of the differential ionization rate as a function of the photoelectron energy and it depends on whether or not the nondipole effects are included. The number of parentheses-like structures increases with the increase of β_0 and for values $\beta_0 > 5$ a.u. the nondipole effects are significant for most values of the photoelectron energy and emission angle.

Moreover, the photoelectron momentum distribution strongly depends on the ellipticity of the driving field. Assuming that β_0 is not too large, the photoelectrons are predominantly emitted in the $p_x p_y$ plane regardless of the field ellipticity. However, the increase of the ellipticity lead to the suppression of the low- and middle-energy electrons and the structure exhibited by the parameter $\delta_{\mathbf{p}i}(n)$ is not visible for the driving field with large ellipticity ($\varepsilon > 0.3$).

In addition to the direct electrons we also analyzed the rescattered electrons. The numerical calculations necessary to obtain the photoelectron energy spectra are time consuming even for the laser-field parameters for which β_0 is close to one. Solving the corresponding system of the saddle-point equations we have found that its solutions can be classified in a similar way as in the dipole approximation. The so-called backward-scattering solutions mainly contribute in the medium- and high-energy parts of the spectra. We presented the partial contributions of these solutions to the differential ionization rate as well as their coherent sum together with the result obtained using the numerical integration. The results obtained using the SP method reproduce effectively the results obtained using the numerical integration. This allows us to get accurate values of the differential ionization rate for a given value of the emission angle and a given range of the photoelectron energy without performing time-consuming numerical calculations.

ACKNOWLEDGMENTS

We gratefully acknowledge support by the Ministry for Science, Higher Education, and Youth, Canton Sarajevo, Bosnia and Herzegovina. We also acknowledge support by the Alexander von Humboldt Foundation and by the Deutsche Forschungsgemeinschaft within the Priority Programme Quantum Dynamics in Tailored Intense Fields (QUTIF).

[1] D. B. Milošević and F. Ehlotzky, Scattering and reaction processes in powerful laser fields, Adv. At. Mol. Opt. Phys. **49**, 373 (2003).

[2] L. Schiff, *Quantum Mechanics*, International Series in Pure and Applied Physics (McGraw-Hill, New York, 1968).

[3] J. Maurer and U. Keller, Ionization in intense laser fields beyond the electric dipole approximation: Concepts, methods, achievements and future directions, J. Phys. B **54**, 094001 (2021).

[4] H. R. Reiss, Limits on Tunneling Theories of Strong-Field Ionization, Phys. Rev. Lett. **101**, 043002 (2008); **101**, 159901(E) (2008).

[5] H. R. Reiss, The tunnelling model of laser-induced ionization and its failure at low frequencies, J. Phys. B **47**, 204006 (2014).

[6] N. J. Kylstra, R. M. Potvliege, and C. J. Joachain, Photon emission by ions interacting with short intense laser pulses: Beyond the dipole approximation, J. Phys. B **34**, L55 (2001).

[7] A. Hartung, S. Brennecke, K. Lin, D. Trabert, K. Fehre, J. Rist, M. S. Schöffler, T. Jahnke, L. Ph. H. Schmidt, M. Kunitski, M. Lein, R. Dörner, and S. Eckart, Electric Nondipole Effect in Strong-Field Ionization, Phys. Rev. Lett. **126**, 053202 (2021).

[8] C. I. Moore, J. P. Knauer, and D. D. Meyerhofer, Observation of the Transition from Thomson to Compton Scattering in Multiphoton Interactions with Low-Energy Electrons, Phys. Rev. Lett. **74**, 2439 (1995).

[9] D. D. Meyerhofer, J. P. Knauer, S. J. McNaught, and C. I. Moore, Observation of relativistic mass shift effects during high-intensity laser-electron interactions, J. Opt. Soc. Am. B **13**, 113 (1996).

[10] A. Ludwig, J. Maurer, B. W. Mayer, C. R. Phillips, L. Gallmann, and U. Keller, Breakdown of the Dipole Approximation in Strong-Field Ionization, Phys. Rev. Lett. **113**, 243001 (2014).

[11] J. Maurer, B. Willenberg, J. Daněk, B. W. Mayer, C. R. Phillips, L. Gallmann, M. Klaiber, K. Z. Hatsagortsyan, C. H. Keitel, and U. Keller, Probing the ionization wave packet and recollision dynamics with an elliptically polarized strong laser field in the nondipole regime, Phys. Rev. A **97**, 013404 (2018).

[12] B. Willenberg, J. Maurer, B. W. Mayer, and U. Keller, Subcycle time resolution of multi-photon momentum transfer in strong-field ionization, Nat. Commun. **10**, 5548 (2019).

[13] M. Klaiber, K. Z. Hatsagortsyan, and C. H. Keitel, Above-threshold ionization beyond the dipole approximation, Phys. Rev. A **71**, 033408 (2005).

[14] A. S. Titi and G. W. F. Drake, Quantum theory of longitudinal momentum transfer in above-threshold ionization, Phys. Rev. A **85**, 041404(R) (2012).

[15] S. Brennecke and M. Lein, High-order above-threshold ionization beyond the electric dipole approximation, J. Phys. B **51**, 094005 (2018).

[16] S. Brennecke and M. Lein, High-order above-threshold ionization beyond the electric dipole approximation: Dependence on the atomic and molecular structure, Phys. Rev. A **98**, 063414 (2018).

[17] S. V. B. Jensen, M. M. Lund, and L. B. Madsen, Nondipole strong-field-approximation Hamiltonian, Phys. Rev. A **101**, 043408 (2020).

[18] R. Kahvedžić and S. Gräfe, Strong-field approximation with leading-order nondipole corrections, Phys. Rev. A **105**, 063102 (2022).

[19] C. T. L. Smeenk, L. Arissian, B. Zhou, A. Mysyrowicz, D. M. Villeneuve, A. Staudte, and P. B. Corkum, Partitioning of the Linear Photon Momentum in Multiphoton Ionization, Phys. Rev. Lett. **106**, 193002 (2011).

[20] A. Hartung, S. Eckart, S. Brennecke, J. Rist, D. Trabert, K. Fehre, M. Richter, H. Sann, S. Zeller, K. Henrichs *et al.*, Magnetic fields alter strong-field ionization, Nat. Phys. **15**, 1222 (2019).

[21] P.-L. He, K. Z. Hatsagortsyan, and C. H. Keitel, Nondipole Time Delay and Double-Slit Interference in Tunneling Ionization, Phys. Rev. Lett. **128**, 183201 (2022).

[22] P.-L. He, M. Klaiber, K. Z. Hatsagortsyan, and C. H. Keitel, Nondipole Coulomb sub-barrier ionization dynamics and photon momentum sharing, Phys. Rev. A **105**, L031102 (2022).

[23] E. Hasović, M. Busuladžić, A. Gazibegović-Busuladžić, D. B. Milošević, and W. Becker, Simulation of above-threshold ionization experiments using the strong-field approximation, Laser Phys. **17**, 376 (2007).

[24] E. Clementi and C. Roetti, Roothaan-Hartree-Fock atomic wavefunctions: Basis functions and their coefficients for ground and certain excited states of neutral and ionized atoms, $Z \leqslant 54$, At. Data Nucl. Data Tables **14**, 177 (1974).

[25] A. D. McLean and R. S. McLean, Roothaan-Hartree-Fock atomic wave functions Slater basis-set expansions for $Z = 55-92$, At. Data Nucl. Data Tables **26**, 197 (1981).

[26] C. F. Bunge, J. A. Barrientos, and A. V. Bunge, Roothaan-Hartree-Fock ground-state atomic wave functions: Slater-type orbital expansions and expectation values for $Z = 2-54$, At. Data Nucl. Data Tables **53**, 113 (1993).

[27] A. A. Radzig and B. M. Smirnov, *Reference Data on Atoms, Molecules, and Ions* (Springer, Berlin, 1985).

[28] G. F. Gribakin and M. Y. Kuchiev, Multiphoton detachment of electrons from negative ions, Phys. Rev. A **55**, 3760 (1997).

[29] S. Chelkowski, A. D. Bandrauk, and P. B. Corkum, Photon Momentum Sharing between an Electron and an Ion in Photoionization: From One-Photon (Photoelectric Effect) to Multiphoton Absorption, Phys. Rev. Lett. **113**, 263005 (2014).

[30] P.-L. He, D. Lao, and F. He, Strong Field Theories beyond Dipole Approximations in Nonrelativistic Regimes, Phys. Rev. Lett. **118**, 163203 (2017).

[31] D. B. Milošević and W. Becker, Improved strong-field approximation and quantum-orbit theory: Application to ionization by a bicircular laser field, Phys. Rev. A **93**, 063418 (2016).

[32] A. Kramo, E. Hasović, D. B. Milošević, and W. Becker, Above-threshold detachment by a two-color bicircular laser field, Laser Phys. Lett. **4**, 279 (2007).

[33] E. Hasović, A. Kramo, and D. B. Milošević, Energy- and angle-resolved photoelectron spectra of above-threshold ionization and detachment, Eur. Phys. J.: Spec. Top. **160**, 205 (2008).

[34] W. Becker and D. B. Milošević, Above-threshold ionization for very low electron energy, J. Phys. B **48**, 151001 (2015).

[35] D. B. Milošević, Forward- and backward-scattering quantum orbits in above-threshold ionization, Phys. Rev. A **90**, 063414 (2014).

[36] A. Jašarević, E. Hasović, R. Kopold, W. Becker, and D. B. Milošević, Application of the saddle-point method to strong-laser-field ionization, J. Phys. A: Math. Theor. **53**, 125201 (2020).

[37] D. Habibović, A. Gazibegović-Busuladžić, M. Busuladžić, and D. B. Milošević, Characteristics of the molecular above-threshold ionization by a bichromatic elliptically polarized field with co-rotating components, J. Phys. B **55**, 085601 (2022).

[38] D. B. Milošević, G. G. Paulus, D. Bauer, and W. Becker, Above-threshold ionization by few-cycle pulses, J. Phys. B **39**, R203 (2006).

[39] M. Klaiber, E. Yakaboylu, H. Bauke, K. Z. Hatsagortsyan, and C. H. Keitel, Under-the-Barrier Dynamics in Laser-Induced Relativistic Tunneling, Phys. Rev. Lett. **110**, 153004 (2013).

[40] S. Chelkowski, A. D. Bandrauk, and P. B. Corkum, Photon-momentum transfer in multiphoton ionization and in time-resolved holography with photoelectrons, Phys. Rev. A **92**, 051401(R) (2015).

[41] H. Ni, S. Brennecke, X. Gao, P.-L. He, S. Donsa, I. Březinová, F. He, J. Wu, M. Lein, X.-M. Tong *et al.*, Theory of Subcycle Linear Momentum Transfer in Strong-Field Tunneling Ionization, Phys. Rev. Lett. **125**, 073202 (2020).

[42] M. Klaiber, K. Z. Hatsagortsyan, and C. H. Keitel, Subcycle time-resolved nondipole dynamics in tunneling ionization, Phys. Rev. A **105**, 053107 (2022).

[43] D. B. Milošević, E. Hasović, M. Busuladžić, A. Gazibegović-Busuladžić, and W. Becker, Intensity-dependent enhancements in high-order above-threshold ionization, Phys. Rev. A **76**, 053410 (2007).

[44] D. B. Milošević and W. Becker, Role of long quantum orbits in high-order harmonic generation, Phys. Rev. A **66**, 063417 (2002).

[45] C. F. de Morisson Faria, H. Schomerus, and W. Becker, High-order above-threshold ionization: The uniform approximation and the effect of the binding potential, Phys. Rev. A **66**, 043413 (2002).